Nanoscale

Accepted Manuscript

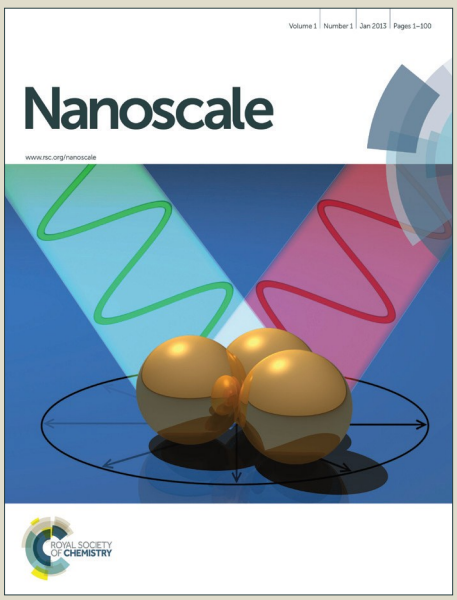

ROYAL SOCIETY OF CHEMISTRY

www.rsc.org/nanoscale

Thermal conductivity of single- and multi-layer phosphorene: A molecular dynamics study

Ying-Yan Zhang *[a], Qing-Xiang Pei *[b], Jin-Wu Jiang *[c], Ning Wei [d], Yong-Wei Zhang [b]

[a] *School of Computing, Engineering and Mathematics, Western Sydney University, Penrith, NSW 2751, Australia*

[b] *Institute of High Performance Computing, A*STAR, Singapore 138632, Singapore*

[c] *Shanghai Institute of Applied Mathematics and Mechanics, Shanghai Key Laboratory of Mechanics in Energy Engineering, Shanghai University, Shanghai 200072, China*

[d] *College of Water Resources and Architectural Engineering, Northwest A&F University, China*

*E-mail: yingyan.zhang@uws.edu.au (YYZ), peiqx@ihpc.a-star.edu.sg (QXP) and jwjiang5918@hotmail.com (JWJ)

Abstract

As a new two-dimensional (2D) material, phosphorene has drawn growing attention owing to its novel electronic properties, such as layer-dependent direct bandgaps and high carrier mobility. Herein we investigate the in-plane and cross-plane thermal conductivities of single- and multi-layer phosphorene, focusing on geometrical (sample size, orientation and layer number) and strain (compression and tension) effects. A strong anisotropy is found in the in-plane thermal conductivity with its value along the zigzag direction being much higher than that along the armchair direction. Interestingly, the in-plane thermal conductivity of multi-layer phosphorene is insensitive to the layer number, which is in strong contrast to that of graphene where the interlayer interactions strongly influence the thermal transport. Surprisingly, tensile strain leads to an anomalous increase in the in-plane thermal conductivity of phosphorene, in particular in the armchair direction. Both the in-plane and cross-plane thermal conductivities can be modulated by external strain; however, the strain modulation along the cross-plane direction is more effective and thus more tunable than that along the in-plane direction. Our findings here are of great importance for the thermal management in phosphorene-based nanoelectronic devices and for thermoelectric applications of phosphorene.

1. Introduction

Recent years have witnessed incredible advances in the research of two-dimensional (2D) materials, in particular, after the discovery of graphene.[1] As the first 2D material, graphene has created unprecedented science sensations due to its novel electronic, thermal and mechanical properties.[2-8] Researchers were thus motivated to explore other 2D materials, such as graphene allotropes,[9-11] silicene,[12-14], hexagonal boron nitride (*h*-BN)[15, 16] and molybdenum disulphide (MoS_2).[17-19]

The most recent 2D material, which has attracted great attention, is phosphorene - the single-layer black phosphorus (see Figure 1).[20-22] Recent theoretical and experimental studies revealed that phosphorene is an anisotropic 2D semiconductor with high carrier mobility,[23] and a large direct band gap about 1.5 eV,[24] making it promising for potential applications in nanoelectronics, such as field-effect transistors and photo-transistors. Phosphorene is also found to have a high figure of merit (ZT value) at room temperature. First-principle calculations show that ZT value is greater than 1.0 at 300 K,[25] and the external tensile strain of 8% can enhance the ZT value in the armchair direction to 2.12.[26] The high ZT value of phosphorene implies its potential applications in thermoelectric devices. Since these applications are closely related to its thermal properties, much effort has thus been devoted to exploring its thermal properties. For example, Fei et al.[25] found that phosphorene exhibits a pronounced spatial-anisotropic lattice thermal conductance and electrical conductance. From the first principles calculations, Qin et al.[27] showed that the thermal conductivity of phosphorene is anisotropic, and the prominent electrical and thermal conducting directions are orthogonal to one another. The computed thermal conductivity at 300 K for the armchair and zigzag directions is 13.65 and 30.15 $Wm^{-1}K^{-1}$, respectively. Using the same method, Jain and McGaughey[28] predicted the thermal conductivity of phosphorene to be 36 and 110 $Wm^{-1}K^{-1}$ along its armchair and zigzag directions. Using first-principle calculation and non-

equilibrium Green's function method, Ong et al.[29] observed a strong anisotropy in thermal conductance of phosphorene, with the thermal conductance along zigzag direction being 40% higher than that along armchair direction at 300K. They also evaluated the effect of tensile strain on the thermal conductance anisotropy and found that a uniaxial tensile strain is able to reduce the thermal conductance in the armchair direction, but increase the thermal conductance in the zigzag direction.

It is worth noting that the previous works[25, 27-29] on the thermal conductivity of phosphorene were based on the first-principles calculations, and thus they used very small samples to generate the linear K matrix (phonon dispersion) and the third-order nonlinear K matrix, based on which they further calculated the thermal conductivity by including phonon-phonon scatterings. Up to now, a detailed study on the thermal conductivity of single-layer phosphorene based on molecular dynamics (MD) simulations is still lacking. Besides, no work has been done on the thermal properties of multi-layer phosphorene. The effects of layer number and mechanical strain on the thermal conductivity of multi-layer phosphorene remain unexplored.

In this work, we perform MD simulations to study the thermal conductivities of single-layer and multi-layer phosphorene in the diffusive transport regime by accounting for the phonon-phonon scattering. The effects of the sample size, lattice orientation, number of layers, and mechanical strain on the thermal conductivity of phosphorene have been investigated.

2. Simulation method

All the MD simulations are performed using LAMMPS package.[30] The Stillinger-Weber (SW) potential parameterized by Jiang[31] is employed to describe the covalent interaction between the phosphorous atoms in phosphorene, while the Lennard-Jones (LJ) potential is

used for the van der Waals (vdW) interaction across different layers in multi-layer phosphorene. The LJ potential is expressed as $V(r_{ij}) = 4\varepsilon\left[(\sigma/r_{ij})^{12} - (\sigma/r_{ij})^{6}\right]$, where r_{ij} is the distance between atoms i and j; ε and σ are the energy and distance constants, respectively. These parameters ($\varepsilon = 0.0132\ eV$ and $\sigma = 3.695$ Å) used in the present MD simulations are obtained from the Universal Force Field.[32] It is noted that the value of σ is not directly provided in the reference. Instead, the distance at which the LJ potential reaches its minimum, r_0, was given. The value of σ is obtained as $\sigma = r_0/(2^{1/6}) = 3.695$ Å. The cutoff distance of the LJ potential is 15 Å. The multi-layer phosphorene is stacked in the A-B sequence, which is the most stable stacking sequence with the lowest energy.[33]

The thermal conductivity is obtained by using the non-equilibrium molecular dynamics (NEMD).[34] The simulation model is divided into 100 slabs along the length direction, with the heat source and sink each taking one of the slabs. As illustrated in Figure 2a, the heat source and sink slabs are located at the middle and the two ends of the model, respectively. Periodic boundary conditions are applied in all the three directions. The initial relaxed configuration is equilibrated at 300 K in NPT ensemble for 4×10^5 steps with a time step of 0.5 fs. Then the system is switched to NVE ensemble to conserve the energy. By continuously exchanging the kinetic energies (every 100 time steps) between the hottest atom in the heat sink slab and the coldest atom in the heat source slab in NVE ensemble, the heat flux J due to the exchange of kinetic energies is then given.

To make sure that the temperature profile in the heat flux direction has reached steady state before data collection, we have outputted the average temperature profiles every 0.5ns and found that there is little change in the temperature profiles after about 2.5ns, meaning that system has reached steady state. The final thermal conductivity is obtained by averaging data over another 2.5 ns period in the steady state and the error bars are calculated using block averaging approach. The thermal conductivity λ is calculated by using the Fourier law as

$$\lambda = \frac{J}{\partial T/\partial l} \quad (1)$$

where $\partial T/\partial l$ is the temperature gradient along the heat flux direction (see Figure 2b).

In essence, thermal energy is the energy of atomic vibration, which can be characterized by the vibration power spectrum or vibrational density of states (VDOS) in the frequency domain. To explain the underlying physics of the thermal transport property of phosphorene, the VDOS was computed by taking Fourier transform of the velocity autocorrelation function (VAF) of all the atoms as:

$$P(\omega) = \frac{1}{\sqrt{2\pi}} \int_0^\tau e^{i\omega t} \langle v(t)v(0) \rangle dt \quad (2)$$

where $P(\omega)$ is the total VDOS at frequency ω, the integration period $\tau = 0.05\, ns$, $\langle v(t)v(0) \rangle$ is the VAF and the bracket denotes the ensemble average of all the atoms. For polarized VDOS, the VAF is calculated as $\langle v_x v_x + v_y v_y \rangle$ and $\langle v_z v_z \rangle$ for in-plane and out-of-plane VDOS, respectively.

3. Results and discussion

3.1. In-plane thermal conductivity

3.1.1. Effect of sample size and orientation

We first performed MD simulations to study the effects of sample size and lattice orientation on the in-plane thermal conductivity of single-layer phosphorene. Simulation samples are generated with the length varying from 20 to 100 nm and the same width of 20 nm. We have tested the effect of the sample width on the simulation results, and found that an increase in the sample width from 20 to 100 nm has minor effect on the obtained thermal conductivity along the sample length direction. The thermal conductivity λ along the zigzag and armchair directions of phosphorene is computed for different sample lengths so as to explore the size and orientation effects. Our simulation results show that the thermal conductivity of

phosphorene in the two chiral directions under consideration increases with the sample length. Taking the thickness of phosphorene as 5.24 Å,[31] the thermal conductivity of 30 nm and 100 nm-long phosphorene along the zigzag direction is $\lambda_{30} = 6.857$ and $\lambda_{100} = 17.01$ $Wm^{-1}K^{-1}$, respectively. Along the armchair direction, the thermal conductivity is $\lambda_{30} = 2.866$ and $\lambda_{100} = 5.759$ $Wm^{-1}K^{-1}$, respectively. Our NEMD simulations clearly show that the thermal conductivity is strongly size and orientation dependent.

In addition to the phonon-phonon scattering, the phonon scattering also occurs at the heat source and sink when the sample size is smaller than the phonon mean free path (MFP). For a sample with a length smaller than the MFP, the thermal conductivity is affected by the system size. With increasing sample size, the scattering effect at the heat source and sink gradually diminishes, giving rise to the gradual increase in the thermal conductivity. In order to extract the effective MFP, l, and the thermal conductivity of infinitely long phosphorene, λ_∞, an inverse fitting procedure is employed.[35-37] In this procedure, the relationship between λ^{-1} and L^{-1} is expressed as

$$\lambda^{-1} = \lambda_\infty^{-1}\left(\frac{2l}{L} + 1\right) \quad (3)$$

From Figure 3, the thermal conductivity λ_∞ along the zigzag and armchair directions is found to be 42.553 and 9.891 $Wm^{-1}K^{-1}$, respectively, which are comparable to those obtained by Qin et al. (30.15 and 13.65 $Wm^{-1}K^{-1}$).[27] Based on Eq. (3), the corresponding MFP values are found to be l = 39.48 and 18.87 nm, respectively, which are much smaller than that of graphene (i.e. 775 nm).[38] This also explains the much smaller thermal conductivity of phosphorene. Different from the thermal conductivities of other 2D materials, such as graphene,[39] silicene[36, 40] and MoS_2,[41-44] the thermal conductivity of phosphorene shows a strong anisotropy with a factor of 4.3, in line with the previous results obtained by other

researchers.[27, 28] This strong anisotropy in the thermal conductivity of phosphorene may be attributed to its puckered configuration in the armchair direction.[29, 45]

3.1.2. Effect of layers

In order to examine the layer effect, we performed MD simulations on the in-plane thermal conductivity of multi-layer phosphorene by varying the number of layers from 2 to 7. The multi-layer phosphorene sample has in-plane dimensions of 20x20 nm^2 and the layers are stacked in the stable A-B stacking sequence. The in-plane thermal conductivities of multi-layer phosphorene along both the zigzag and armchair directions with different layer numbers are illustrated in Figure 4. It is seen that thermal conductivity is around 5.57 $Wm^{-1}K^{-1}$ and 2.32 $Wm^{-1}K^{-1}$ in the zigzag and armchair directions, respectively. Apparently, the thermal conductivities along these two in-plane directions are insensitive to the number of layers. This layer number-independent thermal conductivity is in sharp contrast to that of graphene, as it was shown thermal conductivity in multi-layer graphene decreases with increasing layer number.[46-48]

To further examine this layer-independent thermal conductivity, we calculated the VDOS for the multi-layer phosphorene. The VDOS is calculated in NVE ensemble after the system is relaxed in NPT ensemble at 300 K, but before the heat flux is imposed. It is clearly seen from Figure 5 that the profiles of VDOS for multi-layer phosphorene with different numbers of layers show a high level of similarity. In particular, the peaks in the low and high frequency regions occur around 5 and 12.5 THz for all the cases.

The underlying physical origin behind this layer-independent thermal conductivity of multi-player phosphorene can be explained as follows. Unlike graphene with only one-atom thickness, the atoms in single-layer phosphorene are arranged in two sub-layers and formed puckered geometry as clearly illustrated in Figure 1. This puckered structure in single-layer

phosphorene hinders the out-of-plane (flexural) phonon mode and thus diminishes the layer effect in multi-layer phosphorene.

To further explain this interesting point, we plot the VDOS for both single-layer phosphorene and single-layer graphene in Figure 6. The adaptive intermolecular reactive empirical bond order (AIREBO) potential [49] is used to simulate graphene. It is seen from Figure 6a that the out-of-plane vibration mode (flexural mode) in single-layer graphene makes predominant contribution to the heat conduction in the low frequency range. For multi-layer graphene, the interlayer vdW interactions restrict the flexural mode and thus the thermal conductivity of multi-layer graphene decreases with increasing layer number.[46-48] In contrast to single-layer graphene, the flexural mode in single-layer phosphorene contributes only slightly to the low frequency heat conduction as shown in Figure 6b. Therefore, the increase in the layer number in multi-layer phosphorene and the associated interlayer vdW interactions have negligible effect on the thermal conductivity, resulting in the observed layer-independent characteristics shown in Figure 4.

3.1.3. Strain effect

Mechanical strain has been shown to be an effective means to tune the thermal and electronic properties of nanomaterials.[20, 50-52] Recent MD simulations revealed that the thermal conductivity of graphene and other 2D materials decreases under tensile strain either in the form of uniaxial or biaxial tension.[43, 53, 54] However, an anomalous strain dependence of thermal conductivity in silicene, was reported by Hu et al.[40] and Pei. et al.[36] They found that the thermal conductivity of silicene increases rather than decreases with applied tensile strain. This anomalous strain dependence was attributed to the buckled structure in silicene. As phosphorene also possesses a similar buckled structure in the armchair direction, an interesting question arises: How does the thermal conductivity of phosphorene responds to

the mechanical strain? Below, we address this question by studying the effect of uniaxial strain (both tension and compression) on the thermal conductivity of phosphorene.

MD simulations are performed on single-layer phosphorene sample with a length of 60 nm and a width of 20 nm subjected to different levels of strain along the length direction, which can be either the zigzag or armchair direction. After the structure is fully relaxed, a constant strain rate of $5 \times 10^7 s^{-1}$ is applied along the length direction in NVT ensemble to achieve the desired strain level in the simulation sample. Thereafter, the system is switched to NVE ensemble and a heat flux is applied along the length direction to calculate the corresponding thermal conductivity. Figure 7 shows the effect of uniaxial strain on the thermal conductivity of single-layer phosphorene along both the armchair and zigzag directions. Note that the thermal conductivities shown in Figure 7 are normalized by their corresponding strain-free values, and that the deformed length is used for the calculation of the temperature gradient.

When the phosphorene sample is under compression, the relative thermal conductivity is smaller than 1 for both the zigzag and armchair directions, indicating that compressive strain reduces the thermal conductivity of phosphorene. Similar to graphene, phosphorene undergoes out-of-plane buckling under compressive strain. As the compressive strain increases, the buckling deformation is increased as illustrated in the two insets in Figure 7a, which correspond to the deformed configurations at compressive strain of -0.01 and -0.05, respectively. Since the buckling deformation is able to enhance phonon scattering, consequently, the thermal conductivity of phosphorene decreases, as observed in Figure 7, which is consistent with that of graphene.[54]

When the phosphorene sample is subjected to uniaxial tension, the relative thermal conductivity is greater than 1, implying that the tensile strain exerts a positive influence on

the thermal conductivity. We limit the applied strain along the zigzag direction to 0.04 since the fracture strain of phosphorene along this direction is only around 0.05.[31] The thermal conductivity along the zigzag direction increases slightly when the tensile strain is 0.01. Thereafter, the thermal conductivity reaches a plateau till the strain level of 0.04. However, from the VDOS profiles at different tensile strains shown in Figure 8, it is seen that the tensile strain in the zigzag direction softens both the in-plane and out-of-plane phonon modes, thus depressing the phonon group velocities and hindering the heat conduction. Therefore, this small increase in thermal conductivity along the zigzag direction may be attributed to the tension-induced elongation of the phosphorene sample, which results in higher thermal conductivity due to size effect.

However, the thermal conductivity along the armchair direction increases almost linearly with increasing tensile strain up to 0.08 as shown in Figure 7b. In comparison with Figure 7a, it is readily seen that the tensile strain has more significant effect on the thermal conductivity along the armchair direction. This thermal conductivity enhancement induced by the tensile strain is quite surprising, since it is well known that tensile strain reduces the thermal conductivity of crystal materials. The positive effect produced by the tensile strain for the phosphorene is in sharp contrast to graphene, but similar to silicene.[36, 40] The in-plane and out-of-plane VDOS for the phosphorene sample under tensile strain along the armchair direction are plotted in Figure 9a and 9b, respectively. It is clearly shown that the presence of the tensile strain leads to phonon stiffening in both the in-plane and out-of-plane modes, which facilitates thermal transport. In addition, the phonon stiffening is more obvious in the out-of-plane modes as shown in Figure 9b. Together with the size effect (elongated structures under tensile strain), the thermal conductivity of phosphorene along the armchair direction is thus enhanced remarkably. It is noted that the low frequency modes near 4 THz undergo a small red-shift under tension. Since our MD simulations show that the thermal conductivity

can be enhanced by the mechanical tension, this may indicate a stronger effect from the tension-induced blue-shift of the high frequency phonon modes than the red-shift of the low frequency phonon modes.

3.2. Cross-plane thermal conductivity

Now we study the cross-plane thermal conductivity of multi-layer phosphorene. It is expected that multi-layer phosphorene may have a great potential in nanoelectronic and thermoelectric applications.[55-57] Thus it is of great interest to investigate the thermal transport properties along the cross-plane direction (Z direction) and how the thermal conductivity is changed by the mechanical strain. For this purpose, a 60-layer phosphorene was built with in-plane dimension of 4×4 nm^2 and initial interlayer distance of 5.24 Å. Periodic boundary conditions are applied in all the three directions. The 60-layer structure is long enough for the cross-plane thermal conductivity calculation, as a linear region of the temperature profile is obtained. The interlayer distance after relaxation is about 5.66 Å. The cross-plane compressive or tensile strain is applied on the relaxed structure. The cross-plane thermal conductivity as a function of the cross-plane strain is shown in Figure 10. Here the thermal conductivity is normalized by the thermal conductivity at zero strain. When the strain changes from -0.05 (compression) to 0.05 (tension), the relative thermal conductivity decreases from 2.314 to 0.565, indicating that the cross-plane thermal conductivity can be effectively modulated by the cross-plane strain. This finding is consistent with that for multi-layer graphene under cross-plane strain.[58]

When the multi-layer phosphorene is under cross-plane compression/tension, the relative thermal conductivity is greater/smaller than 1, signifying that the cross-plane compressive/tensile strain enhances/reduces the thermal conductivity. The external strains affect the interlayer interaction strength and then the thermal transport. The compressive

cross-plane strain suppresses the multi-layer phosphorene, reduces the interlayer distance and enhances the interlayer interaction. The stronger interlayer interaction facilitates the heat transport, and thus results in higher thermal conductivity. In contrast, the tensile cross-plane strain increases the interlayer distance, weakens the interlayer interaction and consequently hinders the heat transport.

The interlayer interaction strength can be quantified numerically by the force constant from the second derivative of the interlayer LJ potential with respect to the interlayer distance at different cross-plane strains. The force constant is inversely proportional to the cross-plane strain varying from -0.05 to 0.05 as shown in Figure 11, which corresponds to the variation of the thermal conductivity in Figure 10. In addition, the force constant experiences larger change under cross-plane compression with a larger slope of 0.3541 than 0.3098 under tension. It is evident from Figures 10 and 11 that the cross-plane compression is more effective in adjusting the cross-plane thermal conductivity.

This thermal conductivity modulation by the cross-plane strain can also be explained by the VDOS shown in Figure 12. Apparently, the compressive and tensile cross-plane strain induces phonon stiffening (blue shift) and softening (red shift) of the phonon spectrum, respectively. The phonon stiffening/softening increases/decreases the group velocity, thus leading to an increase/decrease in the thermal conductivity along the cross-plane direction.

4. Conclusions

In summary, we have performed NEMD simulations to study the in-plane and cross-plane thermal conductivities of single- and multi-layer phosphorene. The variation of thermal conductivity with respect to the sample length, orientation, layer number and mechanical strain is systematically examined. From the simulation results, it was found that the phosphorene possesses a strong anisotropy and also strong layer-number independence of in-

plane thermal conductivity due to its puckered structure, which is distinctly different from other 2D materials. Similar to other 2D materials, the in-plane thermal conductivity is dependent on the sample length and mechanical strain. Compared with the in-plane thermal conductivity under uniaxial in-plane strain, the cross-plane thermal conductivity is more sensitive to the cross-plane strain and is thus more tunable by the mechanical strain. Our findings can provide a useful guideline in modulating the thermal properties of phosphorene for its potential applications in thermal management and thermoelectric devices.

Acknowledgement

Y.Y. Zhang is grateful for the computational support provided by Intersect Australia Ltd and 2015 Academic Development Program in Western Sydney University, Australia.

References

1. K. S. Novoselov, A. K. Geim, S. V. Morozov, D. Jiang, Y. Zhang, S. V. Dubonos, I. V. Grigorieva and A. A. Firsov, *Science*, 2004, **306**, 666-669.
2. C. Soldano, A. Mahmood and E. Dujardin, *Carbon*, 2010, **48**, 2127-2150.
3. Q. X. Pei, Y. W. Zhang and V. B. Shenoy, *Carbon*, 2010, **48**, 898-904.
4. T. Y. Ng, J. J. Yeo and Z. S. Liu, *Carbon*, 2012, **50**, 4887-4893.
5. B. Liu, C. D. Reddy, J. W. Jiang, J. A. Baimova, S. V. Dmitriev, A. A. Nazarov and K. Zhou, *Appl. Phys. Lett.*, 2012, **101**, 211909.
6. R. Mas-Balleste, C. Gomez-Navarro, J. Gomez-Herrero and F. Zamora, *Nanoscale*, 2011, **3**, 20-30.
7. N. N. Li, Z. D. Sha, Q. X. Pei and Y. W. Zhang, *J. Phys. Chem. C*, 2014, **118**, 13769-13774.
8. J. Chen, G. Zhang and B. Li, *Nanoscale*, 2013, **5**, 532-536.
9. A. Hirsch, *Nat. Mater.*, 2010, **9**, 868-871.
10. Y. Y. Zhang, Q. X. Pei and C. M. Wang, *Appl. Phys. Lett.*, 2012, **101**, 081909.
11. Y. Y. Zhang, Q. X. Pei, Y. W. Mai and Y. T. Gu, *J. Phys. D: Appl. Phys.*, 2014, **47**, 425301.

12. B. Aufray, A. Kara, S. Vizzini, H. Oughaddou, C. Leandri, B. Ealet and G. Le Lay, *Appl. Phys. Lett.*, 2010, **96**, 183102.
13. Q. X. Pei, Z. D. Sha, Y. Y. Zhang and Y. W. Zhang, *J. Appl. Phys.*, 2014, **115**, 023519.
14. H. Oughaddou, H. Enriquez, M. R. Tchalala, H. Yildirim, A. J. Mayne, A. Bendounan, G. Dujardin, M. A. Ali and A. Kara, *Prog. Surf. Sci.*, 2015, **90**, 46-83.
15. X. Wu, J. Dai, Y. Zhao, Z. Zhuo, J. Yang and X. C. Zeng, *ACS Nano*, 2012, **6**, 7443-7453.
16. Y. F. Gao, X. L. Zhang, Y. H. Jing and M. Hu, *Nanoscale*, 2015, **7**, 7143-7150.
17. A. Splendiani, L. Sun, Y. Zhang, T. Li, J. Kim, C. Y. Chim, G. Galli and F. Wang, *Nano Lett.*, 2010, **10**, 1271-1275.
18. J. W. Jiang, *Nanoscale*, 2014, **6**, 8326-8333.
19. B. Liu, F. Meng, C. D. Reddy, J. A. Baimova, N. Srikanth, S. V. Dmitriev and K. Zhou, *RSC Adv.*, 2015, **5**, 29193-29200.
20. A. S. Rodin, A. Carvalho and A. H. Castro Neto, *Phys. Rev. Lett.*, 2014, **112**, 176801.
21. J. Qiao, X. Kong, Z. X. Hu, F. Yang and W. Ji, *Nat. Commun.*, 2014, **5**, 4475.
22. J. W. Jiang and H. S. Park, *Nat. Commun.*, 2014, **5**, 4727.
23. L. K. Li, Y. J. Yu, G. J. Ye, Q. Ge, X. Ou, H. Wu, D. Feng, X. H. Chen and Y. Zhang, *Nat. Nanotechnol.*, 2014, **9**, 372-377.
24. V. Tran, R. Soklaski, Y. Liang and L. Yang, *Phys. Rev. B*, 2014, **89**, 235319.
25. R. Fei, A. Faghaninia, R. Soklaski, J. A. Yan, C. Lo and L. Yang, *Nano Lett.*, 2014, **14**, 6393-6399.
26. H. Y. Lv, W. J. Lu, D. F. Shao and Y. P. Sun, *Phys. Rev. B*, 2014, **90**, 085433.
27. G. Qin, Q. B. Yan, Z. Qin, S. Y. Yue, M. Hu and G. Su, *Phys. Chem. Chem. Phys.*, 2015, **17**, 4854-4858.
28. A. Jain and A. J. McGaughey, *Sci. Rep.*, 2015, **5**, 8501.
29. Z. Y. Ong, Y. Q. Cai, G. Zhang and Y. W. Zhang, *J. Phys. Chem. C*, 2014, **118**, 25272-25277.
30. S. Plimpton, *J. Compt. Phys.*, 1995, **117**, 1-19.
31. J. W. Jiang, *Nanotechnology*, 2015, **26**, 315706.
32. A. K. Rappe, C. J. Casewit, K. S. Colwell, W. A. Goddard and W. M. Skiff, *J. Am. Chem. Soc.*, 1992, **114**, 10024-10035.
33. J. Dai and X. C. Zeng, *J. Phys. Chem. Lett.*, 2014, **5**, 1289-1293.
34. F. MullerPlathe, *J. Chem. Phys.*, 1997, **106**, 6082-6085.

35. P. K. Schelling, S. R. Phillpot and P. Keblinski, *Phys. Rev. B*, 2002, **65**, 144306.
36. Q. X. Pei, Y. W. Zhang, Z. D. Sha and V. B. Shenoy, *J. Appl. Phys.*, 2013, **114**, 033526.
37. M. Hu and D. Poulikakos, *Nano Lett.*, 2012, **12**, 5487-5494.
38. S. Ghosh, I. Calizo, D. Teweldebrhan, E. P. Pokatilov, D. L. Nika, A. A. Balandin, W. Bao, F. Miao and C. N. Lau, *Appl. Phys. Lett.*, 2008, **92**, 151911.
39. J. Haskins, A. Kinaci, C. Sevik, H. Sevincli, G. Cuniberti and T. Cagin, *ACS Nano*, 2011, **5**, 3779-3787.
40. M. Hu, X. L. Zhang and D. Poulikakos, *Phys. Rev. B*, 2013, **87**, 195417.
41. Y. Q. Cai, J. H. Lan, G. Zhang and Y. W. Zhang, *Phys. Rev. B*, 2014, **89**, 035438.
42. Z. Ding, J. W. Jiang, Q. X. Pei and Y. W. Zhang, *Nanotechnology*, 2015, **26**, 065703.
43. I. Jo, M. T. Pettes, E. Ou, W. Wu and L. Shi, *Appl. Phys. Lett.*, 2014, **104**, 201902.
44. X. J. Liu, G. Zhang, Q. X. Pei and Y. W. Zhang, *Appl. Phys. Lett.*, 2013, **103**, 133113.
45. L. Kou, C. Chen and S. C. Smith, *J. Phys. Chem. Lett.*, 2015, **6**, 2794-2805.
46. S. Ghosh, W. Bao, D. L. Nika, S. Subrina, E. P. Pokatilov, C. N. Lau and A. A. Balandin, *Nat. Mater.*, 2010, **9**, 555-558.
47. L. Lindsay, D. A. Broido and N. Mingo, *Phys. Rev. B*, 2011, **83**, 235428.
48. Z. Wei, Z. Ni, K. Bi, M. Chen and Y. Chen, *Carbon*, 2011, **49**, 2653-2658.
49. S. J. Stuart, A. B. Tutein and J. A. Harrison, *J. Chem. Phys.*, 2000, **112**, 6472-6486.
50. X. Han, H. M. Stewart, S. A. Shevlin, C. R. Catlow and Z. X. Guo, *Nano Lett.*, 2014, **14**, 4607-4614.
51. L. Lindsay, W. Li, J. Carrete, N. Mingo, D. A. Broido and T. L. Reinecke, *Phys. Rev. B*, 2014, **89**, 155426.
52. S. Bhowmick and V. B. Shenoy, *J. Chem. Phys.*, 2006, **125**, 164513.
53. Z. X. Guo, D. Zhang and X. G. Gong, *Appl. Phys. Lett.*, 2009, **95**, 163103.
54. N. Wei, L. Xu, H. Q. Wang and J. C. Zheng, *Nanotechnology*, 2011, **22**, 105705.
55. M. Buscema, D. J. Groenendijk, S. I. Blanter, G. A. Steele, H. S. J. van der Zant and A. Castellanos-Gomez, *Nano Lett.*, 2014, **14**, 3347-3352.
56. Y. Xu, J. Dai and X. C. Zeng, *J. Phys. Chem. Lett.*, 2015, **6**, 1996-2002.
57. J. S. Kim, Y. N. Liu, W. N. Zhu, S. Kim, D. Wu, L. Tao, A. Dodabalapur, K. Lai and D. Akinwande, *Sci. Rep.*, 2015, **5**, 8989.
58. J. Chen, J. H. Walther and P. Koumoutsakos, *Nano Lett.*, 2014, **14**, 819-825.

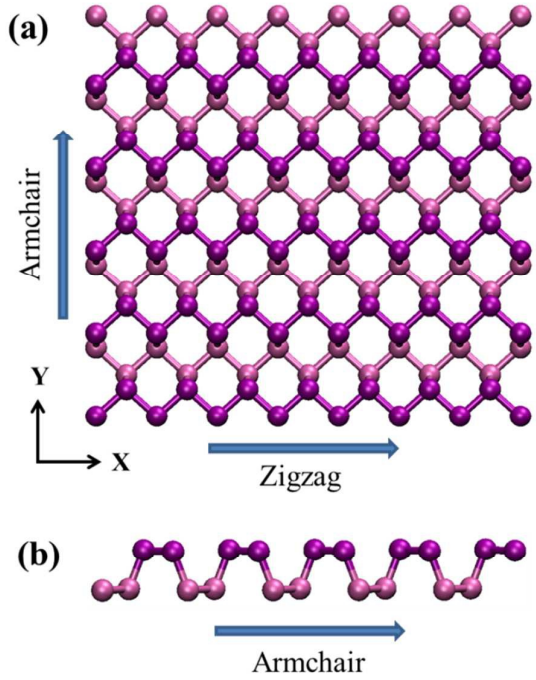

Figure 1. Configuration of single-layer phosphorene. The zigzag and armchair directions are placed along the *x* and *y* directions, respectively.

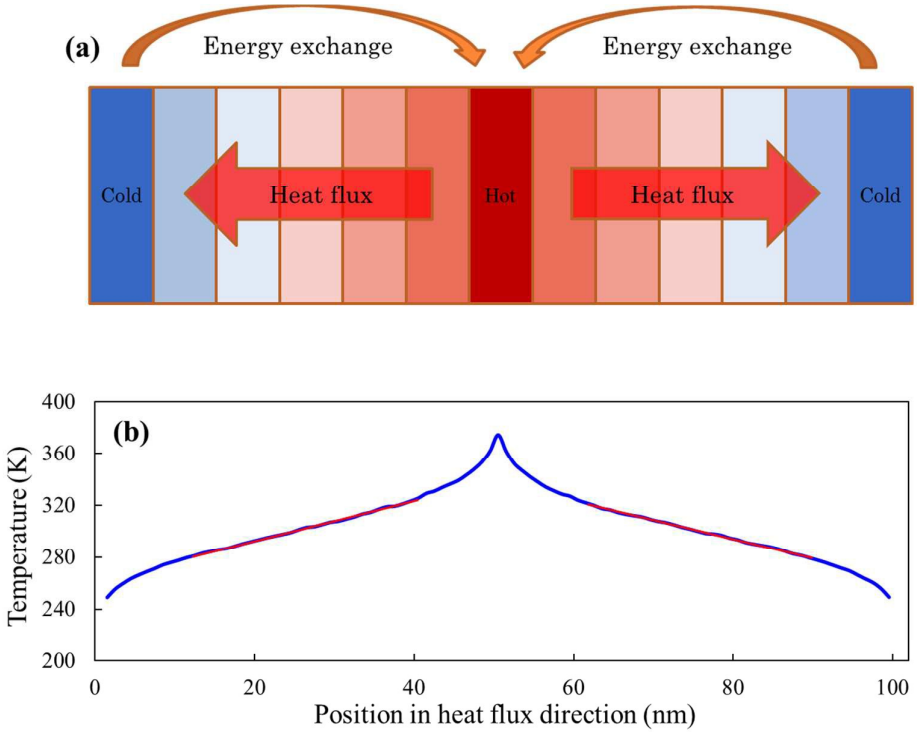

Figure 2. (a) Schematic model for non-equilibrium molecular dynamics simulation. A small amount of heat is repeatedly added into the hot region and removed from the cold regions to create the heat fluxes from the hot region to the cold region. (b) Typical temperature profile along heat flux direction. The temperature gradient is extracted from the linear portions highlighted by the red lines.

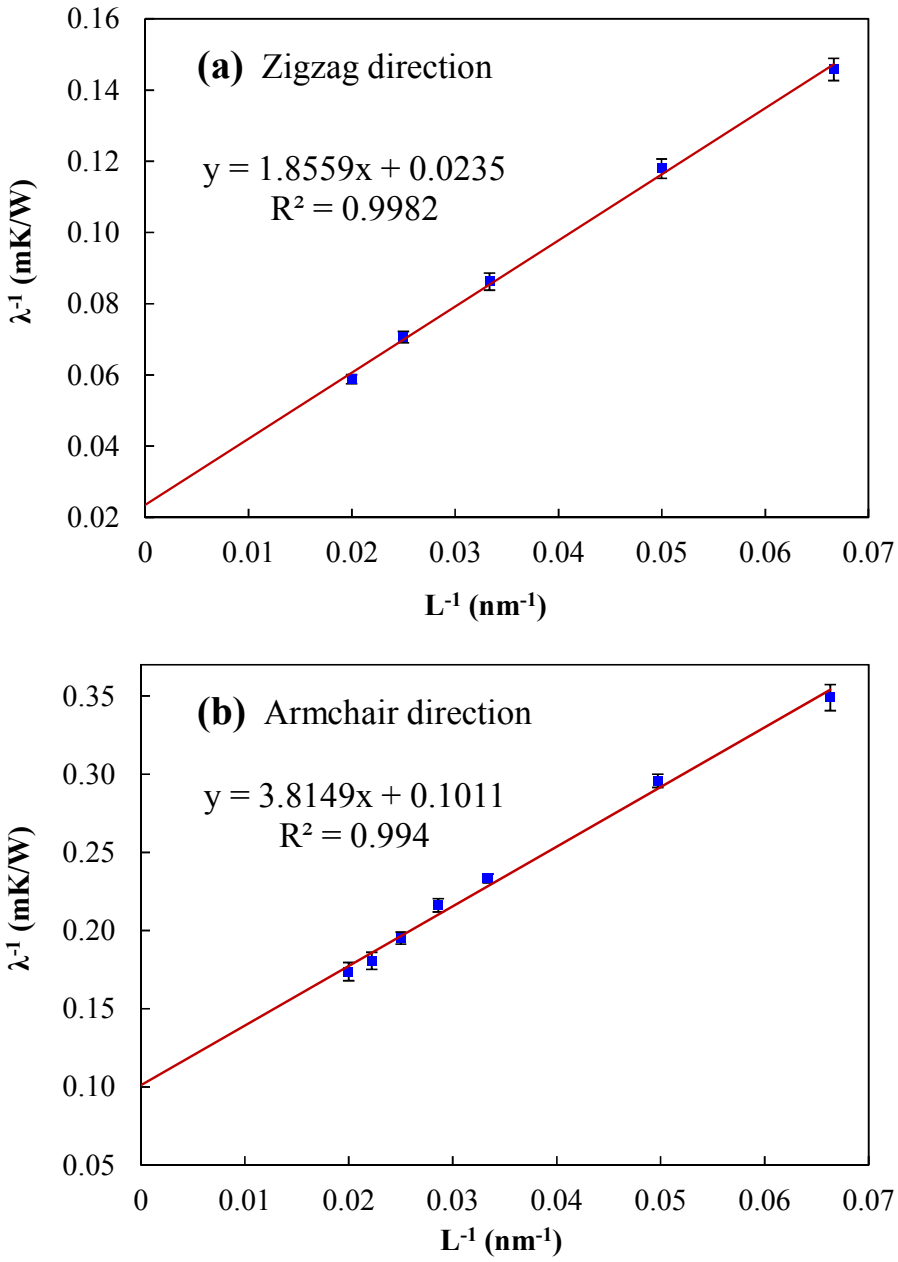

Figure 3. Relationships between inverse length and inverse thermal conductivity of single-layer phosphorene along (a) zigzag and (b) armchair directions. The thermal conductivity at infinitely large phosphorene can be obtained by linear extrapolation at $L^{-1} = 0$.

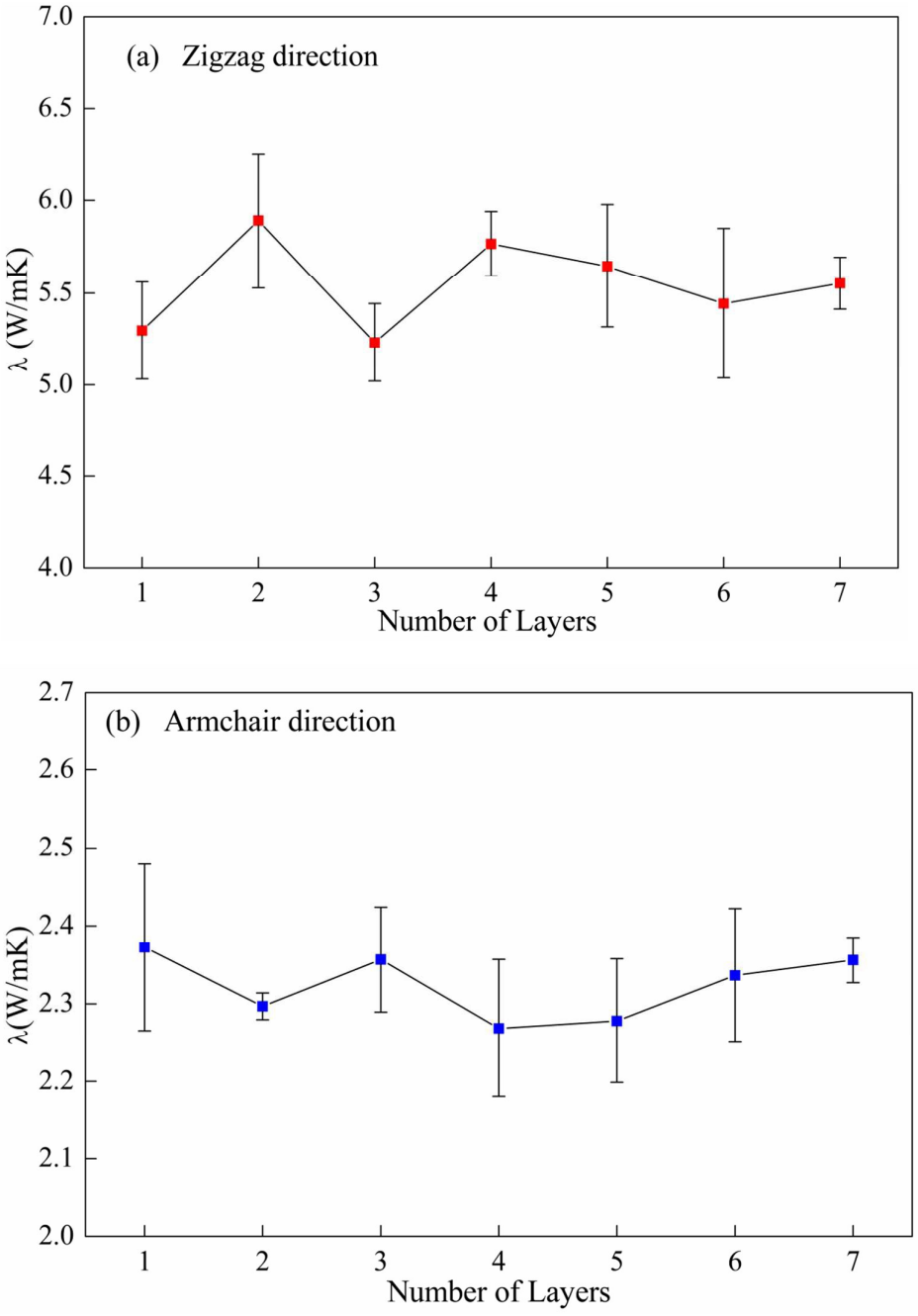

Figure 4. Variation of in-plane thermal conductivity with number of layers in multi-layer phosphorene along zigzag (a) and armchair (b) direction.

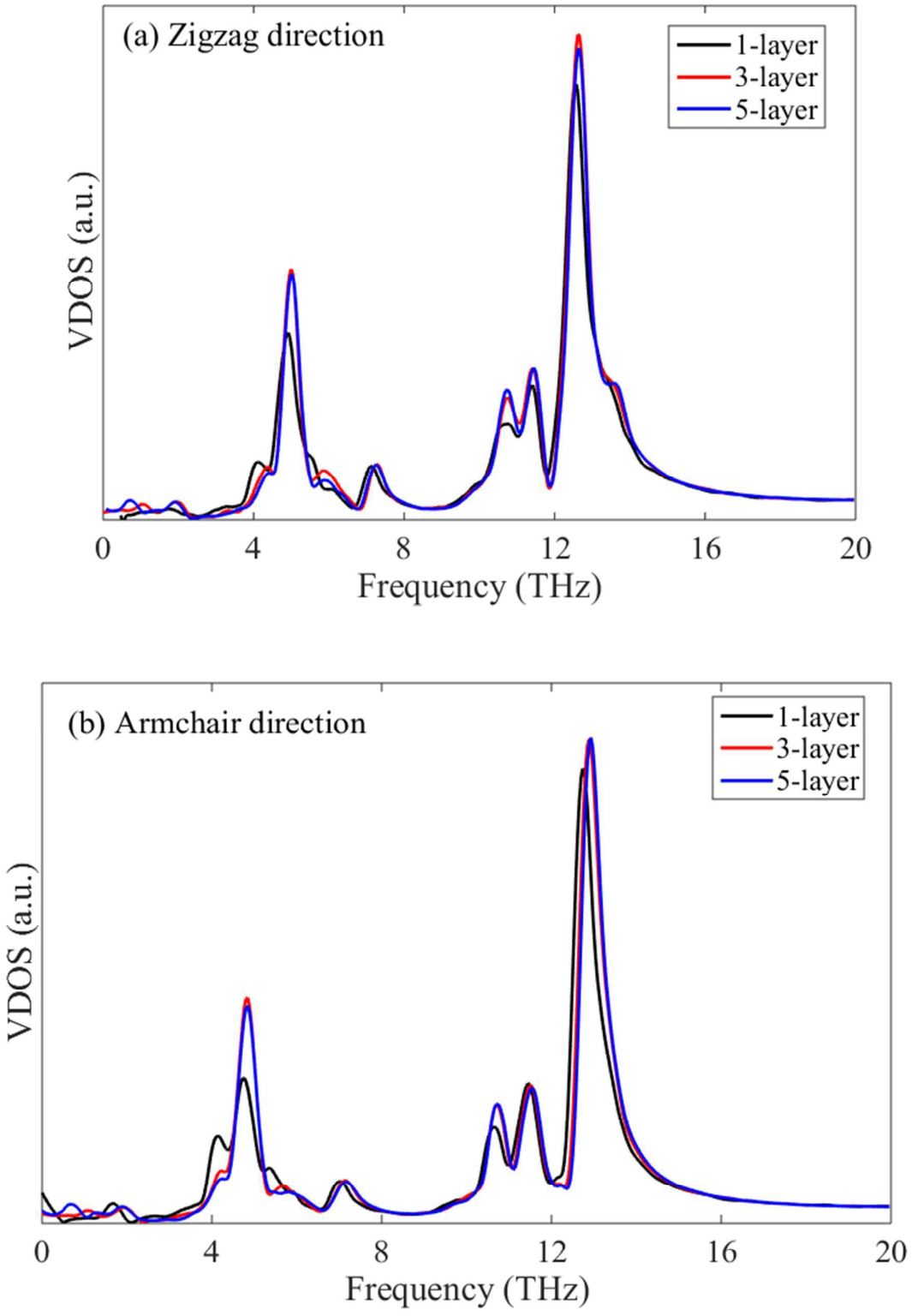

Figure 5. VDOS of single-layer, tri-layer and five-layer phosphorene with heat flux along zigzag (a) and armchair (b) directions.

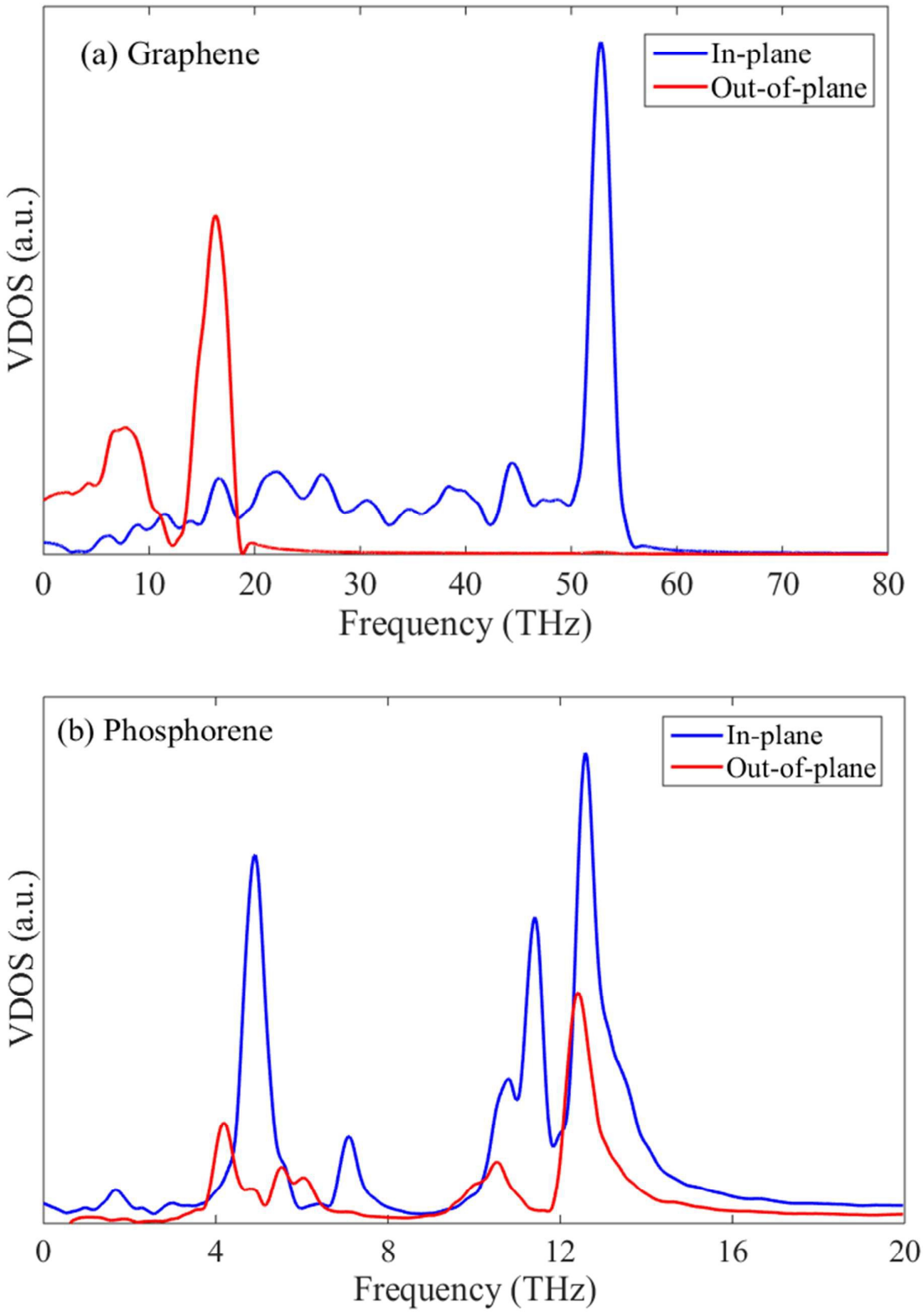

Figure 6. In-plane and out-of-plane VDOS of single-layer graphene (a) and single-layer phosphorene (b).

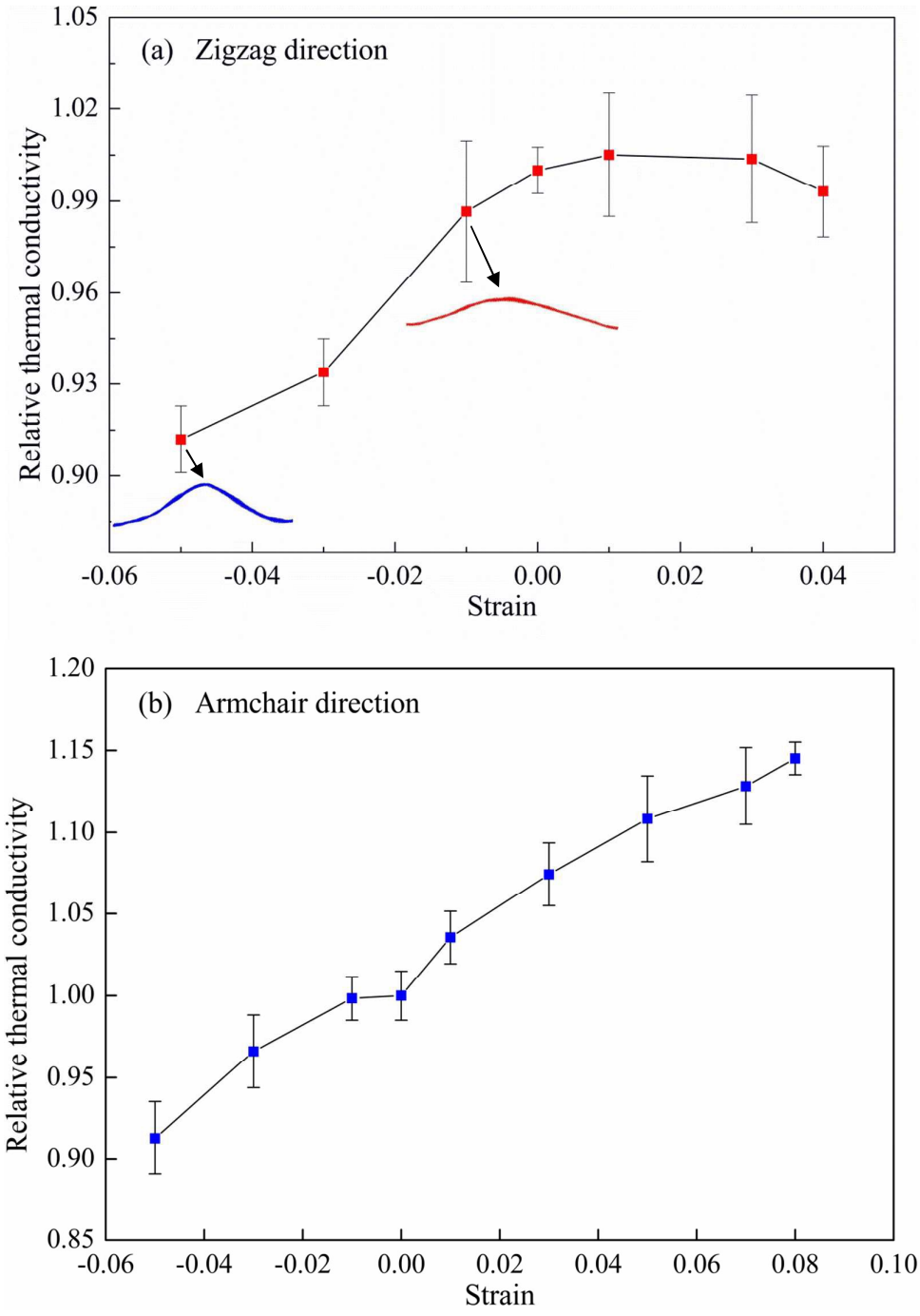

Figure 7. Relative thermal conductivity of single-layer phosphorene as a function of uniaxial strain. The strain is applied in the (a) zigzag and (b) armchair direction. The red and blue curved lines in (a) show the buckled structures at the compressive strains of -0.01 and -0.05, respectively.

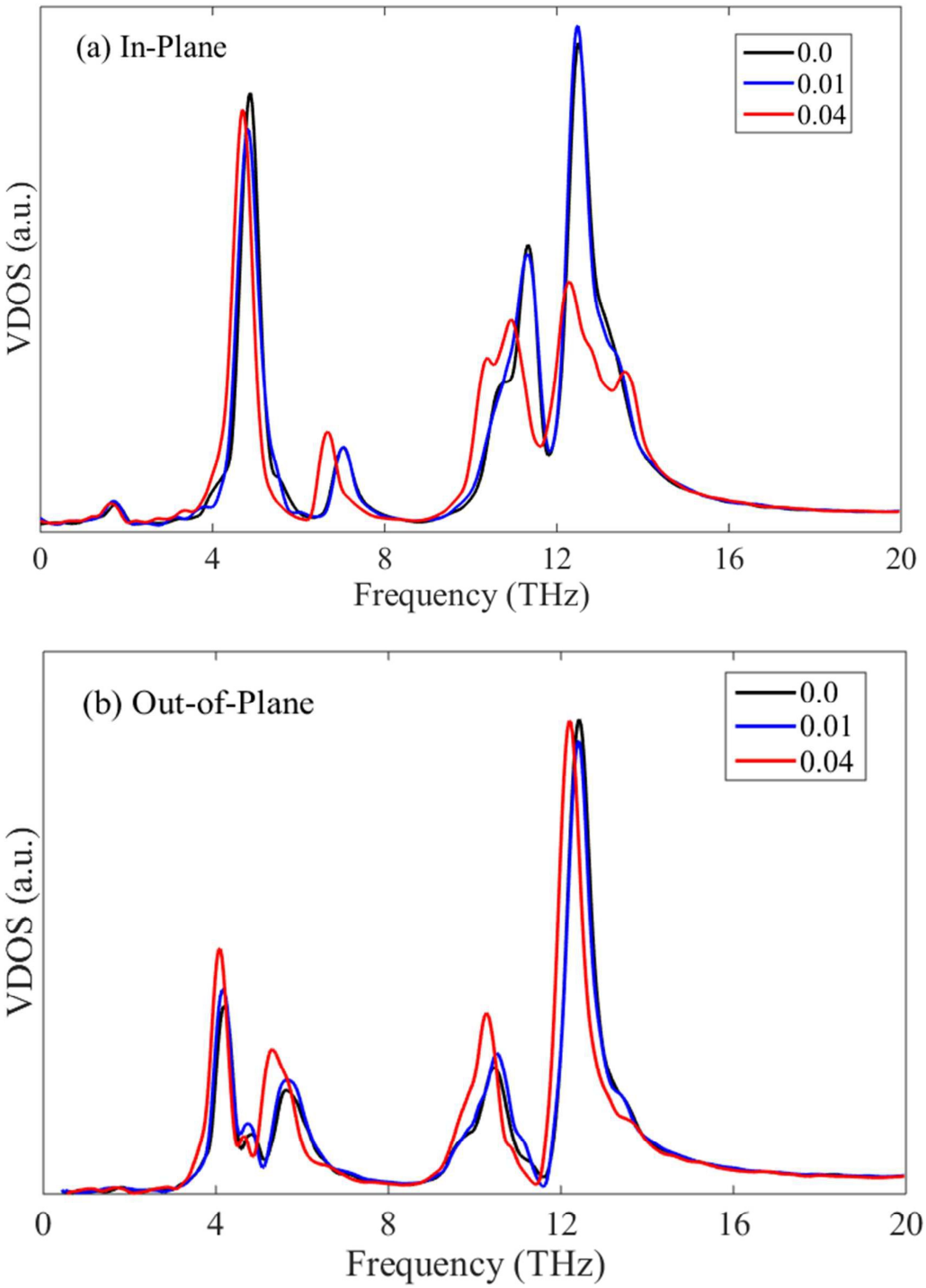

Figure 8. In-plane (a) and out-of-plane (b) VDOS of single-layer phosphorene under tensile strain along the zigzag direction.

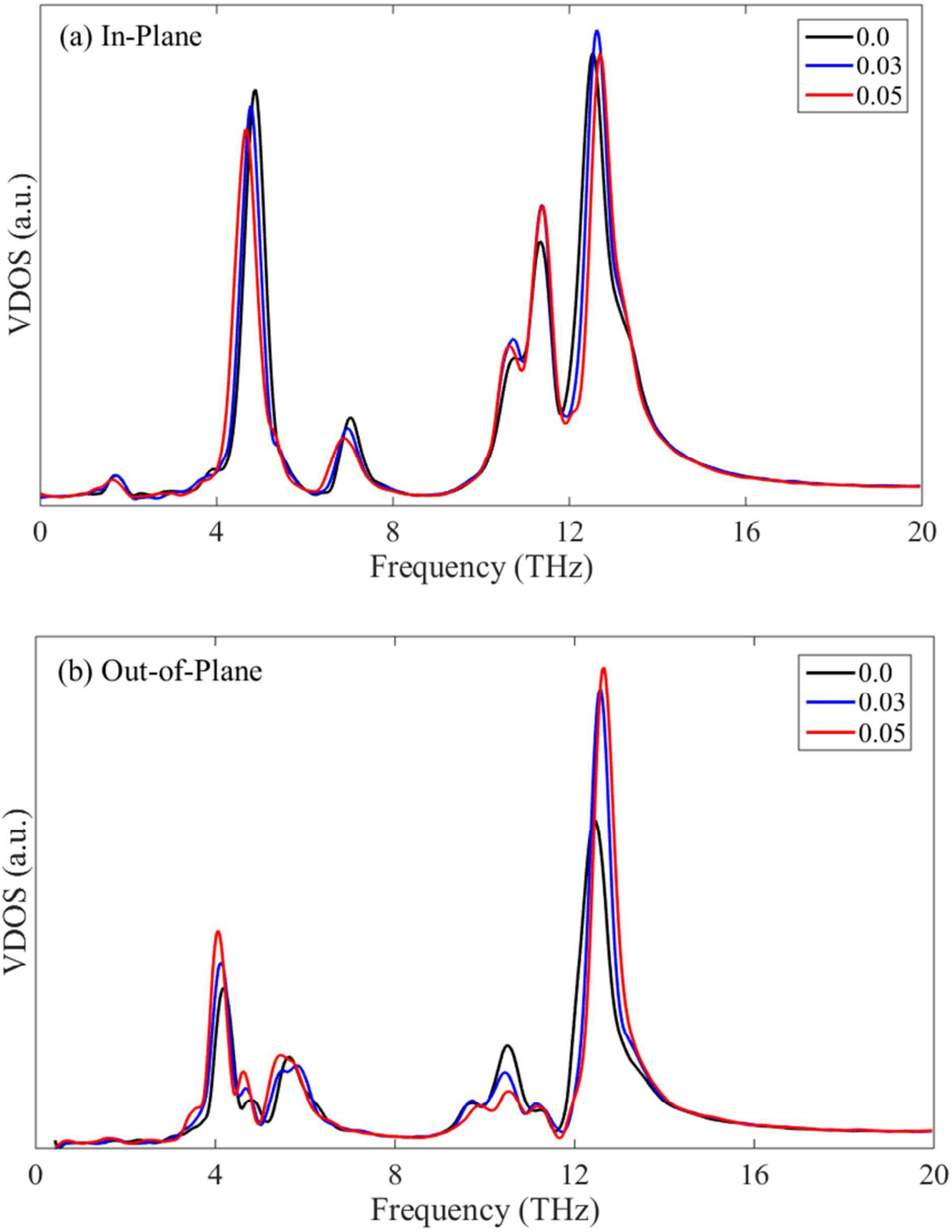

Figure 9. In-plane (a) and out-of-plane (b) VDOS of single-layer phosphorene under tensile strain along the armchair direction.

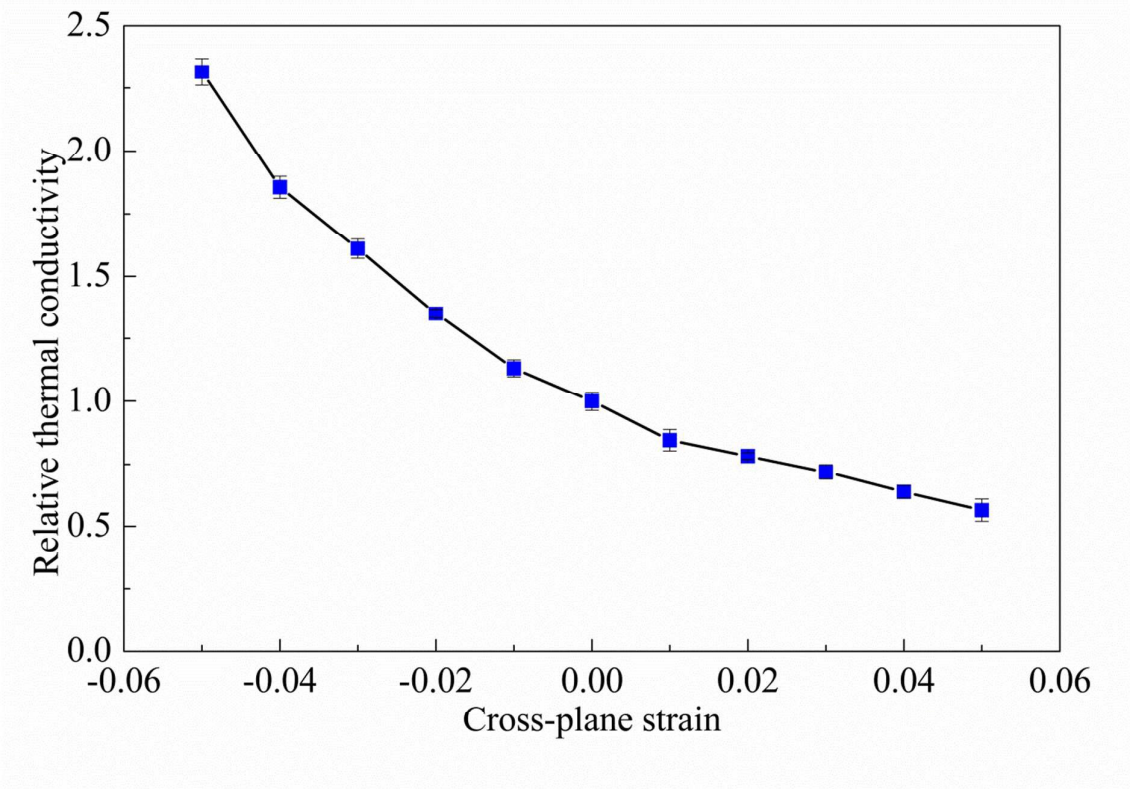

Figure 10. Relative thermal conductivity with respect to strain for multi-layer phosphorene.

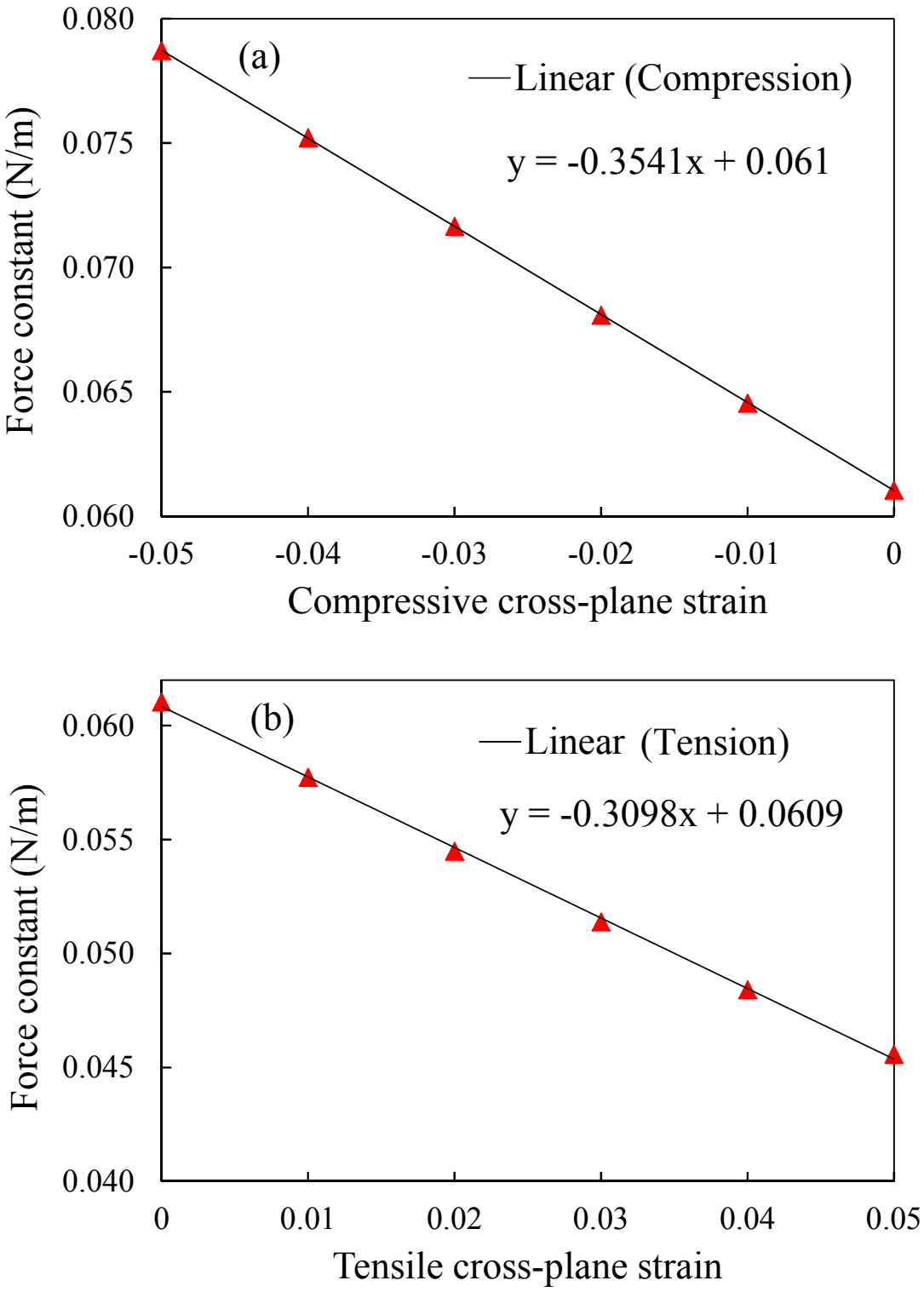

Figure 11. Variation of force constant in multi-layer phosphorene with respect to cross-plane strain.

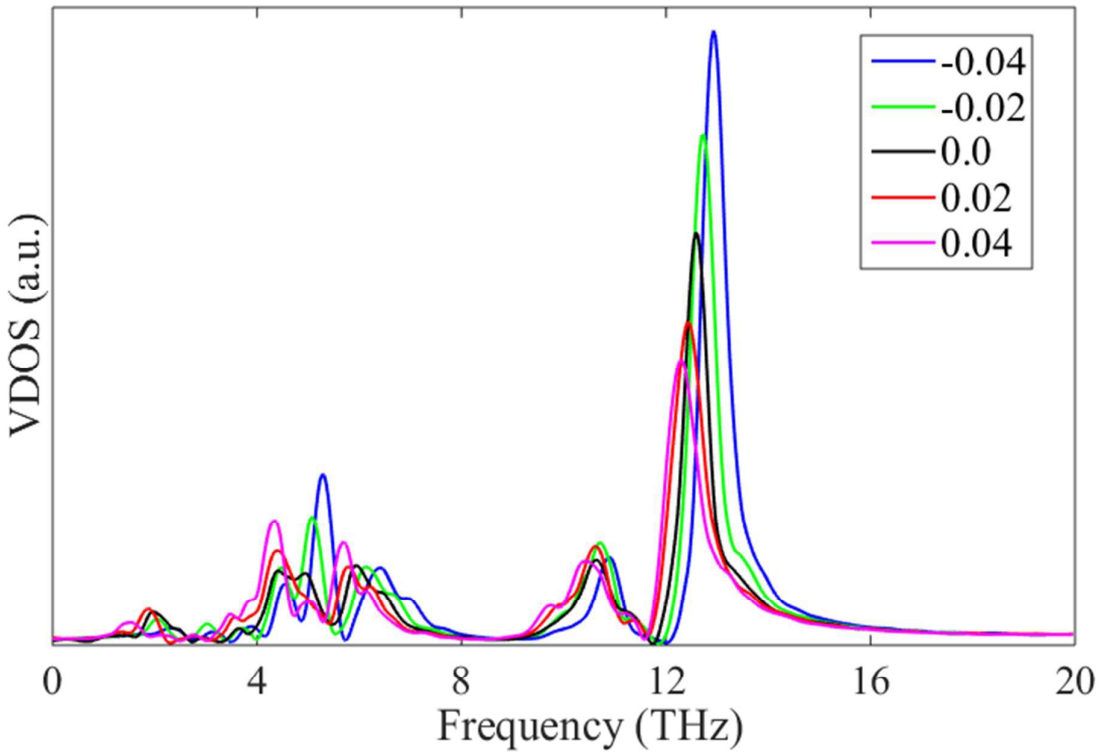

Figure 12. VDOS of multi-layer phosphorene under cross-plane strain.

For the table of contents in the journal

We investigated the in-plane and cross-plane thermal conductivity of single and multi-layer phosphorene using non-equilibrium molecular dynamics simulations.